Dipole-Moment-Based Reciprocity for Practical Desensitization Identification and Mitigation

Shengxuan Xia[®], *Student Member, IEEE*, Hanfeng Wang[®], *Student Member, IEEE*, Yansheng Wang, *Student Member, IEEE*, Zhonghua Wu, *Member, IEEE*, Chulsoon Hwang[®], *Senior Member, IEEE*, and Jun Fan[®], *Fellow, IEEE*

Abstract—Radio frequency interference can degrade the receiving sensitivity of antennas. The interference is usually caused by certain coupling structures, such as layouts without adequate grounding for the radio frequency signal return path. Those structures can be modeled as a set of equivalent dipole moments when they are electrically small. Herein, the dipole moment model-based coupling framework is applied to a practical cellphone design case to devise an engineering solution. The coupling framework incorporates dipole moments as radiation sources and a coupling model based on the reciprocity theorem. Unfortunately, near-field scan probes often lack access to all locations, owing to the complex phone platform structure. A combined measurement-simulation method is used to obtain the field quantities lacking direct access to measurements. The dipole-moment-based coupling framework helps estimate the couplings from different noise sources individually. Thus, the priority of solving for better layout designs can be determined according to the coupling estimations. Furthermore, the physics associated with the reconstructed dipole moment can provide insights and suggest possible mitigation methods. Several practical mitigation methods are discussed, including the suppression of the dominant noise source (reducing/cancelling the radiation or suppressing the specific noise spectrum) and the coupling path to the victim antenna.

Index Terms—Dipole moment, near field scan, radio-frequency (RF) interference, reciprocity, RF desensitization.

I. INTRODUCTION

RADIO frequency (RF) interference widely exists in modern electronic devices. RF noise sources usually originate from integrated circuits (ICs), high-speed channels without adequate shielding, camera modules, etc. In modern electronic devices, although those noise sources may not radiate efficiently in the far-field, thus either preventing the products from passing electromagnetic (EM) compatibility standards or causing electromagnetic interference (EMI) issues, RF antennas can still experience the degradation of sensitivity (RF desensitization).

Manuscript received 21 August 2022; revised 11 December 2022; accepted 20 January 2023. Date of publication 21 June 2023; date of current version 15 August 2023. This work was supported by the National Science Foundation under Grant IIP-1916535. (Corresponding author: Jun Fan.)

Shengxuan Xia, Chulsoon Hwang, and Jun Fan are with the EMC Laboratory, Missouri University of Science and Technology, Rolla, MO 65409 USA (e-mail: sx7c3@mst.edu; hwangc@mst.edu; jfan@mst.edu).

Hanfeng Wang, Yansheng Wang, and Zhonghua Wu are with the Google, Inc., Mountain View, CA 94043 USA (e-mail: hanfeng.wang@gmail.com; yanshengw@google.com; kenzwu@google.com).

Color versions of one or more figures in this article are available at https://doi.org/10.1109/TEMC.2023.3247784.

Digital Object Identifier 10.1109/TEMC.2023.3247784

Given the trend toward designing increasingly compact consumer electronics with wireless communication functions, the noise sources from those ICs or modules tend to have more effective coupling to the RF antennas. Therefore, it has become essential for engineers to efficiently identify the root causes and identify solutions.

Near-field scan measurement is often used in electromagnetic compatibility [1], EMI [2], or RF interference (RFI) applications. A strong near field usually indicates the existence of a significant noise source. More importantly, the measured near field can quantitively characterize noise sources. In practical applications, field measurements are typically acquired by nearfield probes. The electric near-field probes usually have lower measurement accuracy than magnetic near-field probes because of unwanted H-field coupling and common mode coupling [3]. Thus, unless E-field measurement is necessary, H-field measurement is only a typical choice. Moreover, because measuring complex fields (magnitude and phase) introduces greater test complexity, magnitude-only field scanning is usually preferred when possible [4]. A spectrum analyzer or vector network analyzer is used to read the values measured by the near-field probes, and the instrument readings need to be converted into the field strength with a calibration method, such as microstrip-based calibration [5].

The reciprocity theorem effectively aids in the analysis of EM coupling. Huygen's box is one form used to obtain the coupling based on EM fields [6]. Detailed derivations and measurement validations have been given previously [7]. This method also applies to multiple-source cases [8] or special scenarios, such as those in which the noise sources are clamped between two conductor plates [9].

Huygen's box based approach is useful but has two obvious disadvantages: complexity and a lack of physical understanding of the EM coupling. When the physical structure that generates the near field is electrically small, the radiating structure can be approximated as an infinitesimal dipole/loop antenna [10]. An infinitesimal dipole antenna with an excitation of electric current is an electric dipole moment, and an infinitesimal loop antenna can be considered as a dipole driven by a magnetic current, known as a magnetic dipole moment [11]. Furthermore, when scanning on a plane with a certain height, the measured near-field patterns have certain shapes depending on the orientation, type, and amplitude of the equivalent dipole moment. The extracted dipole moments can

0018-9375 © 2023 IEEE. Personal use is permitted, but republication/redistribution requires IEEE permission. See https://www.ieee.org/publications/rights/index.html for more information.

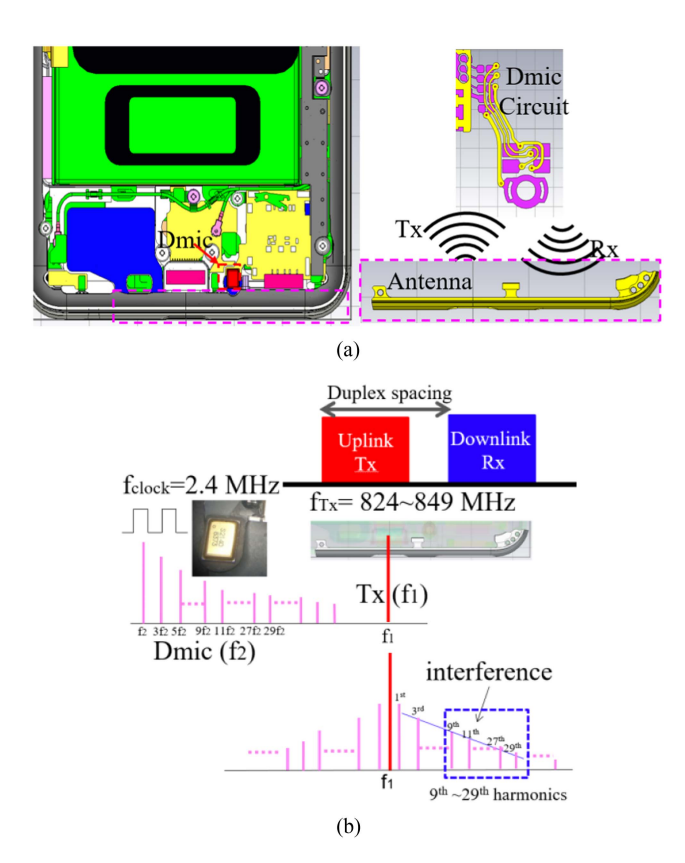


Fig. 1. Demonstration of modulation-involved RF desensitization demonstrations. (a) Round-trip coupling between the RF antenna and the dmic module. (b) Up-conversion of the spectrum by modulation.

effectively model RFI problems by representing complicated noise sources.

A dipole-moment-based coupling framework was developed by using the equivalent dipole moments as a noise radiation source and a coupling model based on the reciprocity theorem. The framework is simple and straightforward, yet provides rigorous physical understanding [12]. Efforts have been made to model dipole moment sources in full-wave simulations [13] and in measurements [14]. Because the near-field pattern of a certain dipole moment always has the same shape, advanced methods such as machine learning can also be used for identifying dipole moment types [15]. A set of equivalent dipole moments can model complicated sources in other applications, such as EMI [16], shielding [17], or far-field [18] scenarios but, nevertheless, are more frequently used in RFI applications. One advantage is that the dipole moment can be extracted with tangential H-field magnitude-only scans [19], thus simplifying the procedures and decreasing time consumption. The other advantage of the dipole-moment-based coupling framework is that it provides better insight into the EM coupling from the source to the victim antenna. For example, the RF current path on a specific USB connector structure has been identified; thus, dipole moment generation is clearly understood [20]. More importantly, effective solutions can be efficiently proposed, such as a simple rotation of the IC placement [21]. RFI problems can become even more complicated when modulation is involved,

such as liquid crystal display clock signals can interfere with the receiving band [22]. Similar issues have been found to be the root causes of RFI due to the modulation of digital microphone (dmic) [23]. The characterization of the modulation may be performed as previously described [24]. In addition, for the measurement of cases involving modulation, the sideband noise may require a duplexer to suppress the high-power transmitting signals for better dynamic range [25]. However, most previous studies aiming to solve real RFI problems have the access to near-field scanning. With the trend toward designing increasingly compact electronic devices, field probes inevitably have limited space for conventional field scanning measurement. Therefore, finding solutions for these scenarios for reference is essential.

Herein, we examined the scenario in which multiple dipole moments are present, and very limited access is available for typical near-field scan measurement. The challenges were conquered on the basis of several assumptions and the information obtained from a changed configuration. Practical solutions showed the high capability of dipole-moment-based reciprocity usage in a complicated case. More importantly, through application of reciprocity for each noise source separately, the priorities of the noise couplings from individual sources were identified. Furthermore, all equivalent dipole moments and coupling paths were clearly determined to understand the mechanism. Efficient and feasible solutions are proposed, together with simulation demonstrations and measurement validation, to demonstrate the improvement.

II. DIPOLE-MOMENT-BASED RECIPROCITY FOR RF COUPLING ESTIMATIONS

A. Brief Introduction to the Problem of Modulation-Involved RF Desensitization

The RF desensitization problem is caused by EM coupling between the dmic module and the RF antenna. Because of the nonideal grounding design near the dmic, the layout becomes a good receiver/radiator structure. According to a previous study [25], three steps cause RF desensitization. 1) The RF antenna radiates the TX signals and couples to the dmic layout. 2) The clock signals are modulated with the captured TX signals in the dmic because of the nonlinearity of the component. 3) The modulated signals (new spectrum) are radiated from the dmic layout and couple back to the RF antenna. As shown in Fig. 1(a), the dmic module is placed very close to the RF antenna so that the round-trip coupling between the antenna and dmic might potentially be sufficient to cause problems. Although the clock signals (fundamental frequency of 2.4 MHz) of the dmic are within a low-frequency range, the up-converted spectrum after modulation with the TX signals falls into the receiving band, as shown in Fig. 1(b).

Furthermore, the actual TX signals radiating from the RF antenna are wideband, and thus, the modulated signals are also wideband. The wideband sideband spectrum tends to be more troublesome than narrowband signals because it contains much higher RF power than a single tone (under the same peak amplitude) and occupies a wider frequency range so that the popping among channels cannot easily skip those with interference.

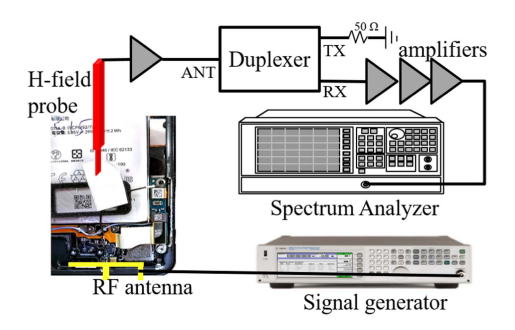


Fig. 2. Near-field scan measurement setup.

B. Noise Source Modeling With Dipole Moments

Dipole-moment-based reciprocity divides the original source-to-victim coupling problem into two parts: source characterization and coupling path modeling. The source characterization involves the extraction of the equivalent dipole moment(s) to represent the noise source(s). The coupling path modeling finds the transfer function from the noise source to the victim antenna. Thus, through application of reciprocity, the coupled voltage on the victim antenna caused by the noise source(s) can be determined by the extracted equivalent dipole moment(s) and the transfer function(s) of the dipole moment(s) to the antenna.

With clear understanding of the mechanism through which the modulated sideband signals interfere with the receiving band, the frequencies of the sideband signals can be determined if the frequency of the TX signal is given. To simplify the measured spectrum analysis, a single tone TX signal from a signal generator was used instead of the actual wideband TX. As shown in Fig. 2, the signal generator produced a 17 dBm sinusoidal wave injected into a cellphone antenna. The dmic module was turned ON. An H-field probe was used to scan the tangential field strength on a certain height plane. The scanning measurement targeted RX frequencies of interest, and the duplexer was added to function as a bandpass filter (specifically for the RX band). The scanned data measured by the spectrum analyzer were converted to field strength with the proper characterization of the field probe [5]. Preliminary sparse scanning results showed that at the target frequencies, the scanned hotspots were located at only two regions: one close to the dmic component and the other near the SIM-flex PCB connector. After the regions of interest were identified, more careful scans were performed in specific locations.

Because of the nonideal grounding design of the dmic portion, the "clock-to-ground" nets formed a loop (see Fig. 1(a), right) that was considered a potential and significant radiator contributing to the EM coupling to the RF antenna nearby. However, the field probe had measurement access to only the region at the connector portion and could not directly characterize the radiated field at the dmic component because the flexible PCB was buried inside the phone with some depth. In addition, the thickness of the dmic metal shielding shell caused the field radiated from the net-formed-loop on the back side to be uncapturable. Instead, the scanned patterns were obtained in the flipped-out configuration. A previous study has shown a "reference" configuration with

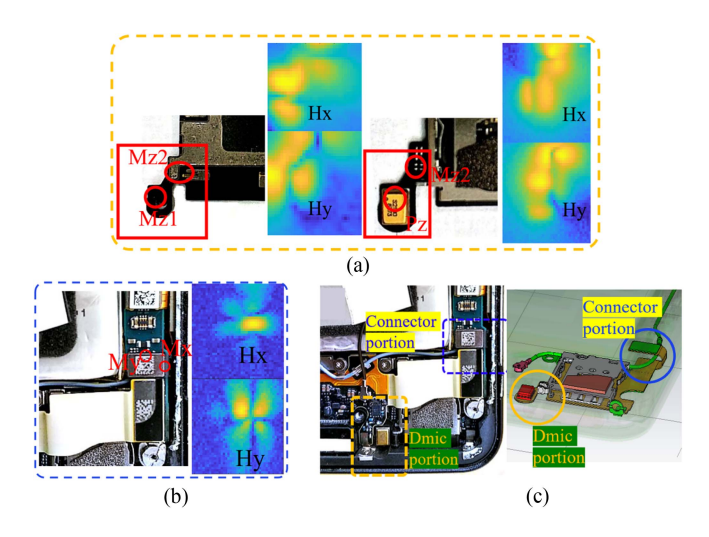


Fig. 3. Scanned H-field patterns, dipole moment types, and locations. (a) Two M_z dipoles and one P_z dipole in the dmic portion. (b) M_x and M_y dipoles in the connector portion. (c) Noise sources on the SIM-flex PCB from two regions.

the SIM-flex flipped outside of the phone, so that both sides of the dmic have access for near-field scan measurement [25], as shown in Fig. 3(a). The connector region was directly measured [see Fig. 3(b)].

The scan measurement with the SIM-flex PCB flipped outside enables identification and understanding of all radiating structures in the dmic portion. With the information on the flexible PCB layout, the scanned patterns, and the alignment of the pattern with the layout/dmic component, the two M_z dipole moments can be understood to be caused by the horizontal loop formed by the clock net and the ground net, whereas the P_z dipole is caused by the vertical displacement current between the dmic die and its metal can. Furthermore, all dipole moments are correlated sources because they all come from the same clock and TX modulated signal/clock harmonics. In addition, when the SIM-flex is placed back inside the cellphone, there is no metal ground beneath the dmic (because it is too close to the antenna, and the design avoids any additional metal structures nearby); therefore, the three dipole moments remain highly correlated and do not have image effect to change the dipoles because of the absence of metal plate beneath the dipole moments [25]. Thus, although the configuration was changed from being flipped out to being placed inside, the sources remained correlated and always shared the same ratios among the three components.

Two types of the spectrum fall within the RX range: the modulated sideband (TX modulation with 9th–20th order clock harmonics) spectrum and the spectrum of high-order (363rd–372nd order) clock harmonics. As discussed, all noise sources are correlated and share the same ratios between one another. Under the condition that the frequency range of interest is below 900 MHz and the entire dimension of the clock net on the SIM-flex PCB is less than 2.5 cm, all sources are in phase for approximations. Notably, the handling for two types of the spectrum differs. For high-order clock harmonics, the RF current originates from the connector side and propagates all way to the dmic component; therefore, the magnitudes of the

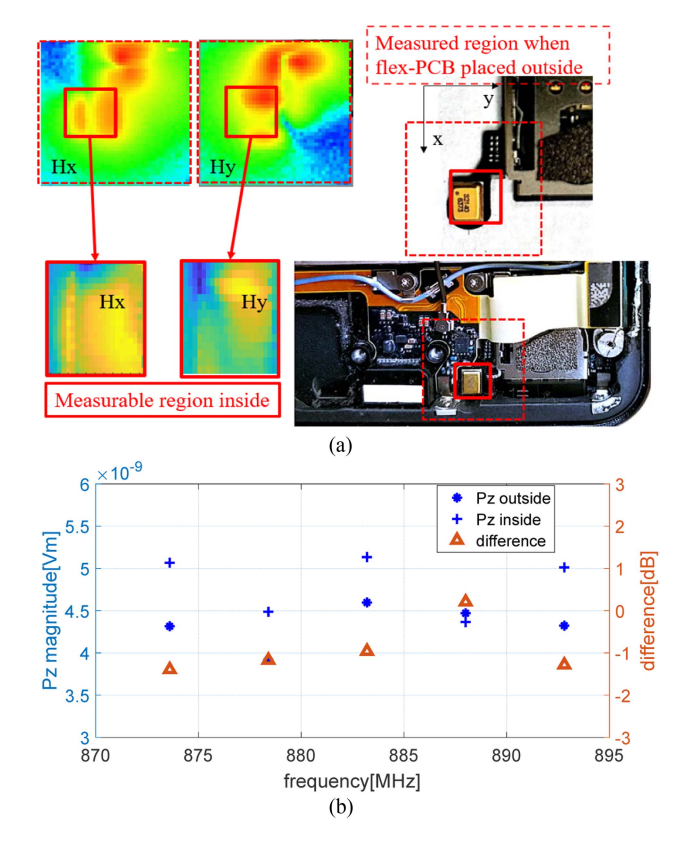


Fig. 4. Rescaling the dipole moment magnitudes with the measurements for two configurations. (a) Flipped-out and original configurations and the corresponding measured field patterns. (b) Measurable P_z dipole (radiating frequency for clock harmonics) extracted from two different configurations.

dipole moments at the dmic portion should be almost the same for both configurations. However, for the modulated sideband spectrum, the first-step couplings from the antenna to the flexible PCB differ for the two configurations. Therefore, unlike the high-order clock harmonics, the generated modulation signals had quite different magnitudes between the two configurations.

Measurements were conducted to verify the assumption that the noise sources caused by the high-order clock harmonics had almost the same magnitudes for both cases. As shown in Fig. 4(a), for the flipped-out case, the P_z dipole moment was extracted from the scanned data on the front side of the dmic. For the original case, a small region remained available for near-field scanning. Although the measurable area inside cannot provide a complete field pattern, the dipole moment still can be extracted with the obtained partial patterns [26]. As shown in Fig. 4(b), the radiating source P_z was nearly the same in both cases with a less than 2 dB difference. The other two M_z dipole moments, when the SIM-flex was placed inside, were also of the same magnitude (within acceptable error), according to the extracted results from the scanned data for the flipped-out case.

Similar procedures were conducted for the modulated signals: two M_z dipoles and one P_z dipole were extracted from the flipped-out case first. Then with the limited measurable region inside, the P_z dipole was extracted from the partial pattern. Based on the study in [23], in the dmic region, all the three dipole

moments are caused by the RF current flowing along the clock net (two M_z dipoles are the horizontal loops and one P_z is the vertical current at the mic component). Small electric dipole (vertical) and its magnetic field strength in the near-field region can be expressed as [27]

$$\boldsymbol{H_{Pz}} \approx \boldsymbol{H_{Pz,\varphi}} = \frac{I_0 l e^{-jkr} \sin \theta}{4\pi r^2} \,\hat{\varphi}$$
 (1)

where I_0 is the electric current flowing along the vertical line with length of l. r is the radial distance from the observation position to the dipole center. While the dipole moment extractions use the scanned magnetic field strengths, thus, when the current amplitude changes to I'_0 , the magnetic field strength follows:

$$|H'_{P_z}|/|H_{P_z}| = I'_0/I_0 = P'_Z/P_z.$$
 (2)

Similarly, for small loop dipole, it satisfies

$$H_{Mz} \approx -j \frac{I_m l e^{-jkr} \cos \theta}{2\omega \mu r^3} \hat{r} - j \frac{I_m l e^{-jkr} \sin \theta}{4\omega \mu r^3} \hat{\theta}$$
 (3)

where I_m is the magnetic current. As the vertically flowing magnetic current is only equivalence but does not exist, Balanis [27] provides the conversion from magnetic current to the real electric current flowing along the loop, expressed as

$$I_m l = j\omega \mu I_0 S \tag{4}$$

where S is the loop area. And similarly, the magnetic field and dipole moment strengths will change following the current as

$$|H'_{M_z}|/|H_M| = I'_m/I_m = I'_0/I_0 = M'_Z/M_z$$
. (5)

Therefore, as all the three dipoles are driven by the same current on the clock net, it is reasonable to make the assumption that the three dipoles always share the same ratios, the two M_z dipoles can be extracted by rescaling as follows:

$$M_{Z1_actual} = M_{Z1_ref} \frac{P_{Z_actual}}{P_{Z_ref}}$$
 (6)

$$M_{Z2_actual} = M_{Z2_ref} \frac{P_{Z_actual}}{P_{Z_ref}}$$
 (7)

where M_{Z1_ref} , M_{Z2_ref} , and P_{Z_ref} are extracted from the measurement for the flipped-out configuration, and P_{Z_actual} is extracted in the original configuration with the partial pattern. As given in Table I, there are three dipole moments used for the modeling of the noise sources at the dmic part, considering both configurations, the four quantities were known from the nearfield scan measurement, and the two unknowns were obtained by (6) and (7). Thus, all noise sources were successfully modeled as in-phase dipole moments with the correct magnitudes. The equivalent modeling for the noise sources was, therefore, solved for this practical application by using dipole-moment-based reciprocity.

C. Coupling Path Modeling

Coupling path modeling characterizes the transfer function from the source to the victim structure. By stimulating the victim structure and measurement of the field at the dipole moment location, the source-to-victim coupling path can be found.

TABLE I EXTRACTED DIPOLE MOMENTS (@873.6 MHz FOR EXAMPLE)

Flipped-out configuration		Original configuration	
Dipole moment	Status and magnitude	Dipole moment	Status and magnitude
$P_{z_{ m ref}}$	Known 3.21e-9 Vm	$P_{z_{\rm _actual}}$	Known 5.13e-9 Vm
$M_{zl_{ m ref}}$	Known 5.65e-12 Am ²	$M_{zI_{ m actual}}$	Unknown 9.04e-12 Am² (scaled)
$M_{z2_{ m ref}}$	Known 4.46e-12 Am²	$M_{z2_ m actual}$	Unknown 7.14e-12 Am² (scaled)

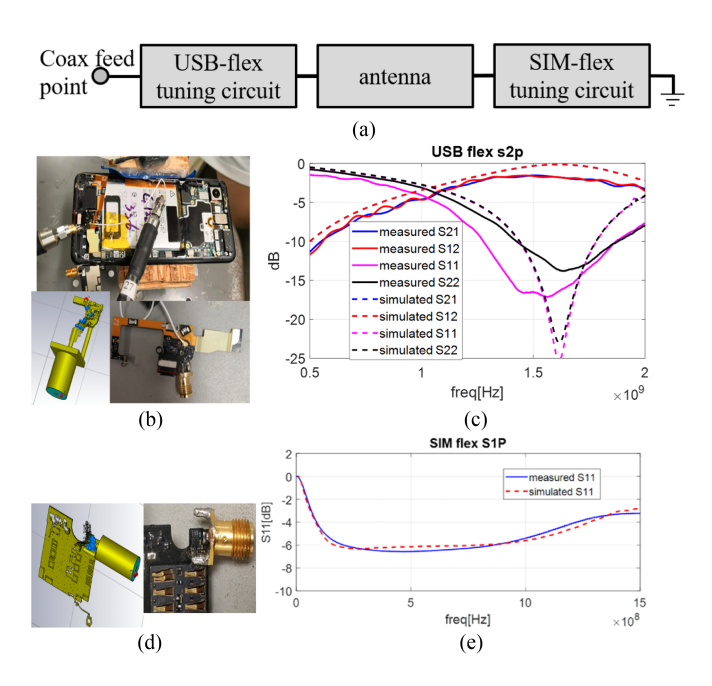


Fig. 5. Modeling of the RF antenna. (a) Connection diagram of the working antenna. (b) Actual USB-flex tuning circuit and full-wave simulation model. (c) Comparison of measured and simulated S-parameters of the USB tuning circuit. (d) Actual SIM-flex tuning circuit and full-wave simulation model. (e) Comparison of measured and simulated S-parameters of the SIM tuning circuit.

However, the field measurement (exciting the victim antenna) has the same challenge as that in equivalent dipole moment extraction. Because the two M_z dipoles are buried inside the cellphone, access is lacking for probing at the equivalent dipole moment locations. Therefore, the coupling path modeling can rely on only full-wave simulations. As shown in Fig. 5(a), the RF antenna has two tuning circuits to adjust the working frequency range for different bands. Thus, the entire antenna module is complicated. Furthermore, not all EM related properties of the materials used in the product are known, and the full-wave simulation requires more effort to tune.

To construct the correct full-wave simulation models of two tuning circuits on the flexible PCBs, the two PCBs were detached

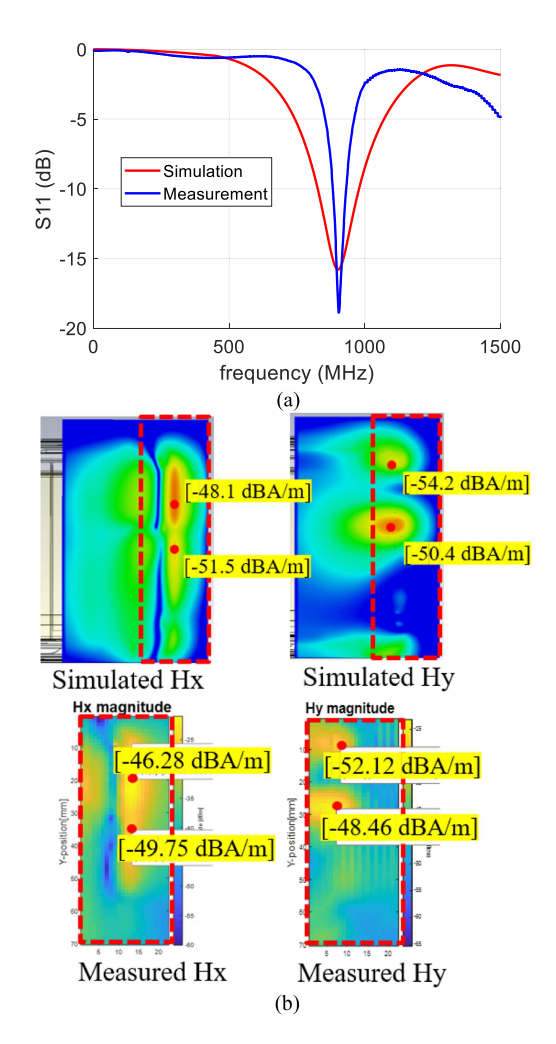


Fig. 6. Performance of the whole antenna module. (a) S_{11} of the antenna. (b) Near-field patterns on the plane above the antenna.

from the phone and soldered with the SMA connectors at the connection points to the antenna structure in Fig. 5(b) and (d). Accordingly, the full-wave simulation models for each PCB had the same connectors attached. After adding all lumped elements and tuning of their values, the simulated *S*-parameters of the circuits eventually matched the measurement results, as demonstrated in Fig. 5(c) and (e). Thus, the full-wave models of both circuits were prepared for the next step.

The SMA connectors were then removed from the full-wave simulation models, and all parts were reassembled according to the connection diagram in Fig. 5(a). Both the S-parameter and the generated near field were then verified for the antenna system. As shown in Fig. 6(a), the full-wave simulation model provided the same resonance frequency of the antenna but did not strictly match the Q-factor. The near field right above the antenna was scanned through measurement and simulation, as shown in Fig. 6(b). The field distributions were nearly identical but the amplitudes had a 2 dB difference, probably because of the inaccurate Q-factor. However, the accuracy of the estimation

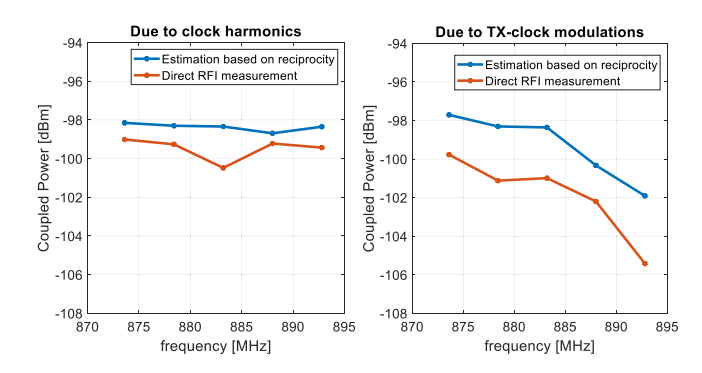


Fig. 7. Correlations of the total EM couplings between direct measurement and reciprocity-based calculations.

of the EM coupling from the noise sources to the antenna was fair.

III. RF COUPLING QUANTIFICATIONS AND ANALYSIS

The noise sources were modeled with equivalent dipole moments with proper handling of the measured data from two configurations. The coupling paths of the sources to the victim antenna were characterized through a combination of measurement and simulation. After both parts were practically solved, dipole-moment-based reciprocity was applied to quantify the couplings and provide further insights.

A. Correlations

The total coupled RF power was directly measured with a previously described setup [25]. The duplexer was used to inject a mimicked TX signal into the antenna and to provide an RF path allowing the RX spectrum to be measured by a spectrum analyzer. The dipole-moment-based reciprocity provided the estimated coupled voltage on the antenna, according to the expression

$$U^{\text{fwd}} = \frac{Z_L}{2U^{\text{rev}}} \left(\sum \overrightarrow{E^{\text{rev}}} \cdot \overrightarrow{P} + \sum \overrightarrow{H^{\text{rev}}} \cdot \overrightarrow{M} \right) \tag{8}$$

where U^{fwd} is the coupled voltage from the noise source to the victim antenna (the original problem), Z_L is the load impedance, and P and M are the extracted dipole moments (electric dipole and magnetic dipole, respectively) from the source characterizations by near scanning. For the coupling path, the incident voltage U^{rev} is the excited voltage on the victim antenna; thus, $\overline{E^{\rm rev}}$ and $\overline{H^{\rm rev}}$ are the electric and magnetic fields at the dipole moment locations sourced from the victim antenna. As discussed in Section II, a total of five dipole moments were present, and the summation of the couplings for the five sources was calculated, as shown in Fig. 7. The dipole-moment-based reciprocity captured the trend of the couplings within a certain error. The correlations of the couplings due to high-order clock harmonics were within a 2 dB error. The estimated couplings due to the modulated signals had a less than 4 dB difference with respect to the directly measured results. These larger differences were probably caused by the rescaling procedures in Section II.

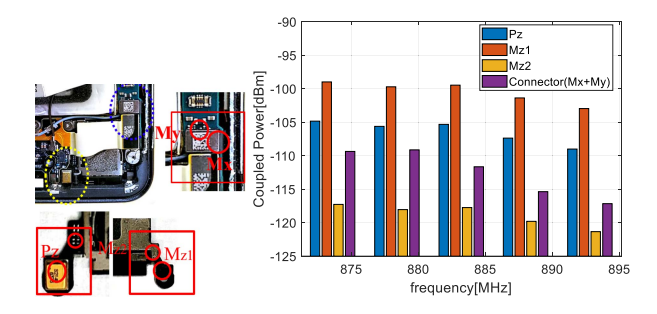


Fig. 8. Individual contributions of the noise sources.

It needs to be emphasized that although the modulated signal couplings have less power than the clock harmonics in real applications, the modulation involved interference is much more troublesome. First, the RFI caused by high-order harmonics is irrelevant to the TX power, but the interference by modulation is proportional to the TX power. Because of the limited TX power level from the signal generator, the input TX in the measurement was only 17 dBm but in actual applications can be as high as 23 dBm. Second, the modulated signals are wideband and always follow the TX channels; therefore, the "contaminated" range cannot be avoided by simply changing the channels.

B. Noise Coupling Contribution Analysis

One of the most important benefits from the dipole-moment-based reciprocity theorem is that the couplings from each individual noise sources can be separated. Thus, the interference contributions can be determined for each problematic structure. Accordingly, engineers can determine the priority of the modifications on each part. For the kth dipole moment source, its coupling contribution to the victim antenna can be expressed as (9) or (10), for magnetic and electric dipole types, respectively.

$$U_k^{\text{fwd}} = \frac{Z_L}{2U^{\text{rev}}} \overrightarrow{H_k^{\text{rev}}} \cdot \overrightarrow{M_k}$$
 (9)

$$U_k^{\text{fwd}} = \frac{Z_L}{2U^{\text{rev}}} \overrightarrow{E_k^{\text{rev}}} \cdot \overrightarrow{P_k}. \tag{10}$$

From (9) and (10), significant noise contributor satisfies two conditions: 1) strong radiation from the dipole source; 2) efficient coupling path to antenna. For example, the two horizontal loops, although the source M_{z1} is not significantly stronger than M_{z2} (see Table I), however, M_{z1} loop is much closer to the antenna and in an efficient coupling orientation, it contributes dominantly and the loop further away is negligible.

The individual coupling contributions after the application of reciprocity in this 5-dipole scenario are shown in Fig. 8. The dominant interference portion is the dmic region instead of the connector region because the coupled RF power from the single Mz1 dipole is 10 dB higher than that from the combination of M_x and M_y in the connector part. The first and second most dominant noise sources are the M_{z1} and P_z dipoles. Therefore, only solving for the layout loop and the metal shell at the dmic is sufficient in practice to suppress RF desensitization.

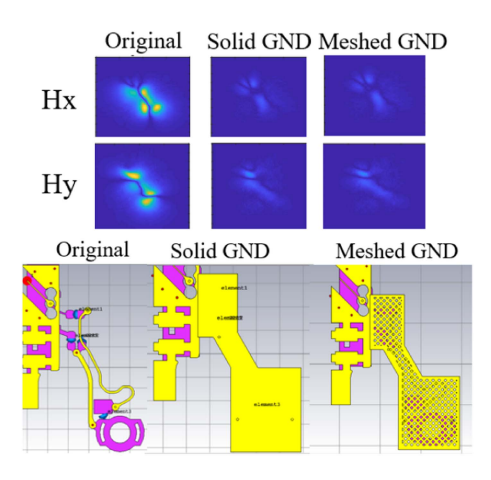


Fig. 9. Near-field changes with additional grounding planes.

IV. PRACTICAL RF DESENSITIZATION MITIGATION METHODS

The physics-based dipole moment extraction provided clear understanding of the radiating structures. Reciprocity theorem calculations indicated the priorities of the mitigation solutions by identifying the dominant coupling contributors. With all preparations, mitigation methods can therefore be devised more efficiently.

A. Suppressing Radiation on Dominant Noise Sources

As indicated by (7), the coupling is proportional to the amplitude of the dipole moment. Therefore, RF desensitization can be decreased if the amplitude of the dominant dipole moment is suppressed. From the physics-based dipole moment extractions, the dominant M_{z1} dipole is caused by the radiating structure formed from the horizontal loop. Thus, a better grounding design can provide a better RF return path to decrease the radiation from the loop. As shown in Fig. 9, by simply adding a piece of ground (either solid or meshed) beneath the dmic circuit layout, the generated near-field strength can be significantly decreased. As a result, the magnitude of the magnetic dipole moment is greatly suppressed, thus resulting in less coupling to the victim antenna.

Although this mitigation method, using a better grounding design, is efficient for solving the desensitization problem, the additional metal piece added near the RF antenna is likely to detune the antenna. Therefore, this solution is not feasible for after-designed products.

B. Coupling Cancellation Method

The two dominant contributors are the P_z and M_{z1} dipoles; therefore, the coupling calculations in (8) can be approximated as

$$U^{\text{fwd}} \approx \frac{Z_L}{2U^{\text{rev}}} \left(\overrightarrow{E_Z^{\text{rev}}} \cdot \overrightarrow{P_Z} + \overrightarrow{H_{Z1}^{\text{rev}}} \cdot \overrightarrow{M_{Z1}} \right)$$
 (11)

where U^{fwd} is the total coupled voltage from the noise source to the victim antenna, and Z_L is the load impedance. $\overrightarrow{P_Z}$ and $\overrightarrow{M_{Z1}}$

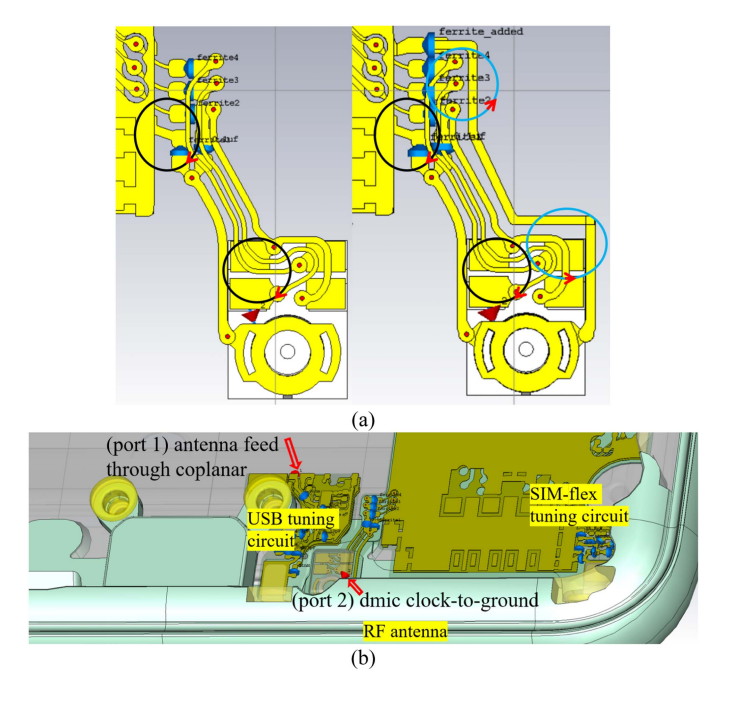


Fig. 10. Cancellation method implementation. (a) dmic circuit layout design: original case (left) and with an additional ground net added (right). (b) Full-wave simulations for the dmic-to-antenna couplings for the two cases.

are the two most dominant dipole moments. $U^{\rm rev}$ is the incident voltage exciting the victim antenna.

Of note, the sources are correlated because they are all originated from the same signal, and the couplings from each individual source will have constant phase differences. In addition, under this frequency and dimension, the phase change has been described to be negligible; therefore, the coupled voltages from the sources will be either in-phase or out-of-phase. Equivalently, the coupled voltages will either additively or subtractively form the ultimate total coupled voltage level.

By taking advantage of this aspect, a "negatively" coupled source can be created to balance the total coupling and suppress RF desensitization. As shown in Fig. 10(a), the M_z dipoles are formed by the horizontal loop beneath the dmic circuit (with the original two M_z dipoles marked as black circles). When another ground net is added at the right side, the RF current can be partially distracted by the new ground net; thus, two additional M_z dipoles are formed (blue circles). Then, when the balanced ground net is added, the total coupling will change to

$$U_{\rm balanced}^{\rm fwd} \approx \frac{Z_L}{2U^{\rm rev}} \left[\overrightarrow{E_Z^{\rm rev}} \cdot \overrightarrow{P_Z} + \overrightarrow{H_{Z1}^{\rm rev}} \cdot \left(\overrightarrow{M_{Z1}'} - \overrightarrow{M_{Z1}''} \right) \right] \ (12)$$

where $U_{\rm balanced}^{\rm fwd}$ is the total coupled voltage for the new configuration, the original $\overrightarrow{M_{Z1}}$ dipole moment is changed to be $\overrightarrow{M_{Z1}'}$ because of the RF current distribution change, the newly formed dipole is $\overrightarrow{M_{Z1}'}$ [note that the current flow directions are opposite, so there is a negative sign in (12)], and because the distance of the two dipoles is extremely small, the magnetic field for both dipole locations can be approximated to be the same as $\overrightarrow{H_{\rm rev}^{\rm rev}}$. To evaluate the feasibility of this balanced loop cancellation

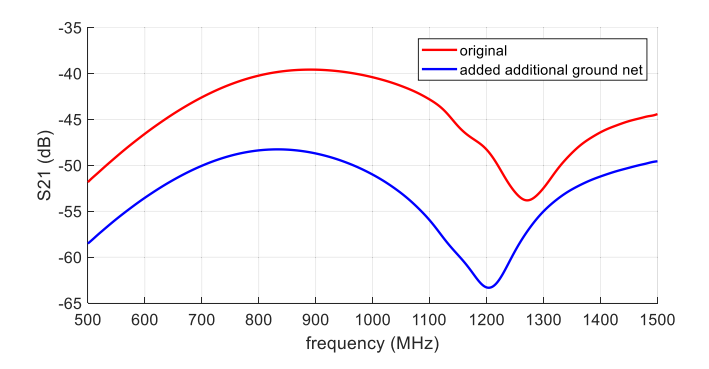


Fig. 11. Simulated S_{21} for the two layout designs of the dmic circuit.

method, the transfer functions for the coupling from the antenna to the dmic circuit were simulated for both configurations. As shown in Fig. 10(b), excitation port 1 was set at the coplanar feeding location before injection into the USB tuning circuit. The entire antenna was simulated to radiate as desired. Because the nonlinearity of the dmic component caused the mixing, the up-converted sideband signals were generated at the dmic component location. Therefore, placing the second port right at the clock-ground pins location of the dmic is reasonable.

Simulations for both configurations were conducted, and the S_{21} (antenna-to-dmic) results are shown in Fig. 11. By adding the extra ground net, the one-way coupling was decreased by 8 dB. Given that the modulation involved RF desensitization was caused by the round-trip coupling, the total suppression on the couplings should be approximately 16 dB.

C. Noise Spectrum Suppression

Beyond the two described methods, because a working dmic needs only a 2.4 MHz clock signal without high requirements on the high-frequency components, ferrite beads can be added to decrease the amplitudes of the unwanted and unnecessary harmonics. As shown in Fig. 12(a), the ferrite beads are placed in series on the clock net. By changing the beads to those with larger impedance, both the 9th–29th harmonics (20–70 MHz) and 363rd–372nd harmonics (869–894 MHz) are significantly suppressed. As a result, the RF desensitization level can be efficiently decreased and can be measured with the setup shown in Fig. 12(b). As shown in Fig. 12(c), decreases of approximately 8 dB on the 363rd–372nd harmonics and approximately 16 dB on the modulated (9th–29th, modulated with TX) harmonics were observed.

D. Summary for RFI Problem Solving

Previous studies have developed a variety of methodologies for solving the RFI problems using near-field scan and reciprocity theory. However, when solving the real industrial problems, time-consuming measurements are done back and forth to improve the measurement qualities. Based on many hands-on measurements experience and debugging process during this study, an efficient workflow is summarized, as Fig. 13

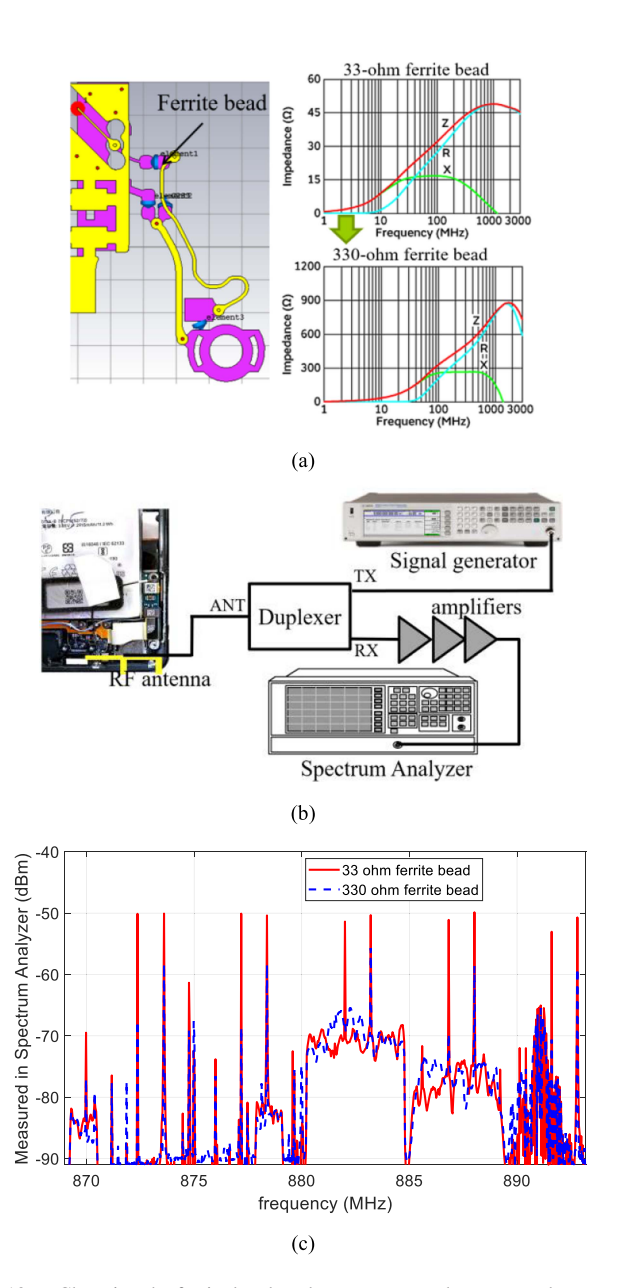


Fig. 12. Changing the ferrite beads to better suppress the unwanted spectrum generation. (a) Changed ferrite bead on the clock net. (b) Validation measurement setup. (c) Measured spectrum before and after changing the ferrite bead.

shows. Appropriate measures need to be taken based on different scenarios for the best fit of a solution to the problem.

V. DISCUSSIONS

This article demonstrated the ability to analyze and solve RFI problems through the application of the dipole-moment-based reciprocity theorem. A sophisticated practical cellphone design was used as an example for demonstration. By taking full advantage of the previous related studies on dipole moment extraction methods, all equivalent dipole moment sources were still successfully modeled even without traditional field scan measurement access. An important advantage of using the reciprocity theorem in scenarios with multiple noise sources is that

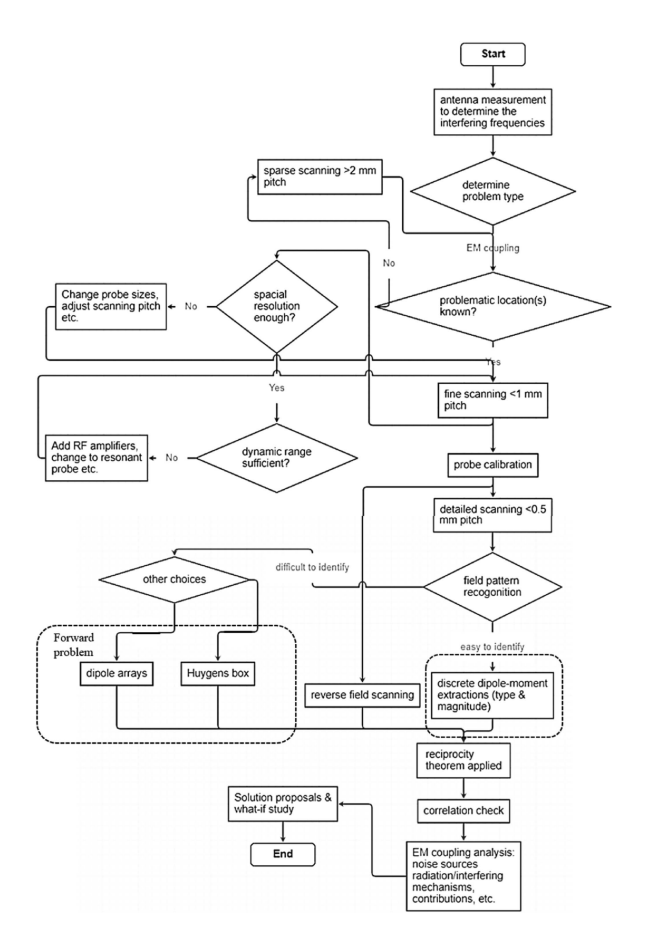


Fig. 13. Practical workflow for solving RFI problems.

the individual contributions can be quantified and ranked for the best engineering efficiency. Furthermore, the physics-based dipole moment extractions can provide insights into exactly which structures are troublesome. Thus, the proposed mitigation solutions are reasonable and effective.

However, the current work has several limitations and lessons as follows.

- 1) The frequency of interest must be relatively low so that the assumption of in-phase noise sources is valid. At higher frequencies, the structure becomes electrically large, and handling remains possible but much more challenging.
- 2) The flipped-out and placed-in configurations share the same sets of dipole moments because of the absence of a conductor beneath the dmic. In more general scenarios, if the configuration is changed, the RF current distributions may change accordingly.
- 3) The slightly poorer accuracy with the rescaled dipole moments might have come from the lack of consideration of the subtle RF current change after the SIM-flex was placed back into the phone.
- 4) Because of the lack of information on materials, extracting the field strengths for such a complicated case from fullwave simulations is typically not recommended because it takes too much effort.

Dipole moment extraction has been extensively studied over the years. However, in solving real-world problems, clearly determining the underlying physics is essential. Only when the dipole moment type is correlated with the extract physical structure causing the radiation can practical solutions come out reasonably and efficiently.

REFERENCES

- E.-X. Liu, W.-J. Zhao, B. Wang, S. Gao, and X.-C. Wei, "Near-field scanning and its EMC applications," in *Proc. IEEE Int. Symp. Electromagn. Compat. Signal/Power Integrity*, 2017, pp. 327–332, doi: 10.1109/ISEMC.2017.8077889.
- [2] Y.-F. Shu and X.-C. Wei, "PCB electromagnetic interference modelling based on reciprocity theorem," in *Proc. IEEE Elect. Des. Adv. Packag. Syst. Symp.*, 2017, pp. 1–3, doi: 10.1109/EDAPS.2017.8276939.
- [3] W. Zhang et al., "Improvement on the accuracy of near-field scanning using tangential electric field probe," in *Proc. IEEE Int. Joint EMC/SI/PI EMC Europe Symp.*, 2021, pp. 370–375, doi: 10.1109/EMC/SI/PI/EMCEurope52599.2021.9559226.
- [4] J. Pan, X. Gao, and J. Fan, "Identifying interference from multiple noise sources using only magnetic near fields," *IEEE Trans. Electromagn. Compat.*, vol. 63, no. 2, pp. 580–588, Apr. 2021, doi: 10.1109/TEMC.2020.3020049.
- [5] J. Zhang, K. W. Kam, J. Min, V. V. Khilkevich, D. Pommerenke, and J. Fan, "An effective method of probe calibration in phase-resolved near-field scanning for EMI application," *IEEE Trans. Instrum. Meas.*, vol. 62, no. 3, pp. 648–658, Mar. 2013.
- [6] H. Wang, V. Khilkevich, Y.-J. Zhang, and J. Fan, "Estimating radio-frequency interference to an antenna due to near-field coupling using decomposition method based on reciprocity," *IEEE Trans. Electromagn. Compat.*, vol. 55, no. 6, pp. 1125–1131, Dec. 2013, doi: 10.1109/TEMC.2013.2248090.
- [7] J. Pan et al., "Radio-frequency interference estimation using equivalent dipole-moment models and decomposition method based on reciprocity," *IEEE Trans. Electromagn. Compat.*, vol. 58, no. 1, pp. 75–84, Feb. 2016, doi: 10.1109/TEMC.2015.2496210.
- [8] Y. Sun, B.-C. Tseng, H. Lin, and C. Hwang, "RFI noise source quantification based on reciprocity," in *Proc. IEEE Symp. Electromagn. Compat.*, *Signal Integrity Power Integrity*, 2018, pp. 548–553, doi: 10.1109/EM-CSI.2018.8495187.
- [9] L. Zhang et al., "Radio-frequency interference estimation for multiple random noise sources," *IEEE Trans. Electromagn. Compat.*, vol. 64, no. 2, pp. 358–366, Apr. 2022, doi: 10.1109/TEMC.2021. 3117845.
- [10] C. A. Balanis, Antenna Theory: Analysis and Design. Hoboken, NJ, USA: Wiley, 1997.
- [11] A. Taaghol and T. K. Sarkar, "Near-field to near/far-field transformation for arbitrary near-field geometry, utilizing an equivalent magnetic current," *IEEE Trans. Electromagn. Compat.*, vol. 38, no. 3, pp. 536–542, Aug. 1996.
- [12] Q. Huang, T. Enomoto, S. Seto, K. Araki, J. Fan, and C. Hwang, "Accurate and fast RFI prediction based on dipole moment sources and reciprocity," in *Proc. DesignCon*, 2018.
- [13] Q. Huang, Y. Liu, L. Li, Y. Wang, C. Wu, and J. Fan, "Radio frequency interference estimation using transfer function based dipole moment model," in *Proc. IEEE Int. Symp. Electromagn. Compat.*, IEEE Asia-Pacific Symp. Electromagn. Compat., 2018, pp. 115–120.
- [14] G.-Y. Cho, J. Jin, H.-B. Park, H. H. Park, and C. Hwang, "Assessment of integrated circuits emissions with an equivalent dipole-moment method," *IEEE Trans. Electromagn. Compat.*, vol. 59, no. 2, pp. 633–638, Apr. 2017, doi: 10.1109/TEMC.2016.2633332.
- [15] Q. Huang and J. Fan, "Machine learning based source reconstruction for RF desense," *IEEE Trans. Electromagn. Compat.*, vol. 60, no. 6, pp. 1640–1647, Dec. 2018, doi: 10.1109/TEMC.2018.2797132.
- [16] S. Lee et al., "Analytical intra-system EMI model using dipole moments and reciprocity," in *Proc. IEEE Int. Symp. Electromagn. Compat.*, *IEEE Asia-Pacific Symp. Electromagn. Compat.*, 2018, pp. 1169–1173, doi: 10.1109/ISEMC.2018.8393972.
- [17] C. Hwang, J.-D. Lim, G. Y. Cho, H.-B. Park, and H. H. Park, "A novel shielding effectiveness matrix of small shield cans based on equivalent dipole moments for radio-frequency interference analysis," *IEEE Trans. Electromagn. Compat.*, vol. 58, no. 3, pp. 766–775, Jun. 2016, doi: 10.1109/TEMC.2016.2536139.

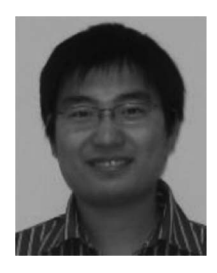
- [18] W. Liu, Z. Yan, J. Wang, Z. Min, and Z. Ma, "An improved equivalent dipole moment source model based on regularization optimization method for near field-far field conversion," *IEEE Access*, vol. 8, pp. 42504–42518, 2020, doi: 10.1109/ACCESS.2020.2976907.
- [19] Q. Huang et al., "A novel RFI mitigation method using source rotation," IEEE Trans. Electromagn. Compat., vol. 63, no. 1, pp. 11–18, Feb. 2021, doi: 10.1109/TEMC.2020.2995828.
- [20] Y. Sun, H. Lin, B.-C. Tseng, D. Pommerenke, and C. Hwang, "Mechanism and validation of USB 3.0 connector caused radio frequency interference," *IEEE Trans. Electromagn. Compat.*, vol. 62, no. 4, pp. 1169–1178, Aug. 2020, doi: 10.1109/TEMC.2019.2925935.
- [21] C. Hwang and Q. Huang, "IC placement optimization for RF interference based on dipole moment sources and reciprocity," in *Proc. Asia-Pacific Int. Symp. Electromagn. Compat.*, 2017, pp. 331–333, doi: 10.1109/APEMC.2017.7975497.
- [22] C. Hwang et al., "Noise coupling path analysis for RF interference caused by LCD noise modulation," in *Proc. IEEE Int. Symp. Electromagn. Com*pat., 2016, pp. 348–352, doi: 10.1109/ISEMC.2016.7571671.
- [23] S. Xia et al., "RFI estimation for multiple noise sources due to modulation at a digital mic using diople moment based reciprocity," in *Proc. IEEE Int. Symp. Electromagn. Compat. Signal/Power Integrity*, 2020, pp. 1–5, doi: 10.1109/EMCSI38923.2020.9743517.
- [24] C. Hwang, D. Pommerenke, J. Fan, T. Enomoto, J. Maeshima, and K. Araki, "Modeling and estimation of LCD noise modulation for radio frequency interference," *IEEE Trans. Electromagn. Compat.*, vol. 59, no. 6, pp. 1685–1692, Dec. 2017, doi: 10.1109/TEMC.2017.2705178.
- [25] C. Hwang, D. Pommerenke, J. Fan, T. Enomoto, J. Maeshima, and K. Araki, "Wideband noise measurement technique in duplex systems for RF interference," *IEEE Trans. Electromagn. Compat.*, vol. 60, no. 4, pp. 1038–1044, Aug. 2018, doi: 10.1109/TEMC.2017.2782673.
- [26] L. Zhang et al., "Accurate RFI prediction of 3D non-planar connector with half magnetic dipole pattern," in *Proc. Joint Int. Symp. Electromagn. Compat.*, Sapporo Asia-Pacific Int. Symp. Electromagn. Compat., 2019, pp. 770–773, doi: 10.23919/EMCSapporo/APEMC44270.2019.8976328.
- [27] C. A. Balanis, Antenna Theory: Analysis and Design. Hoboken, NJ, USA: Wiley, 1997.



Shengxuan Xia (Student Member, IEEE) received the B.S. degree in electrical and computer engineering from the Huazhong University of Science and Technology, Wuhan, China, in 2018. He is currently working toward the Ph.D. degree in electrical engineering with the Electromagnetic Compatibility Laboratory, Missouri University of Science and Technology, Rolla, MO, USA.

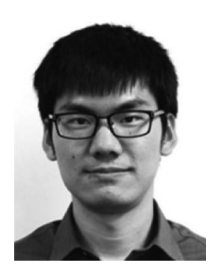
His research interests include radio-frequency interference, desense, radiated emission susceptibility modeling, and hardware security.

Mr. Xia was a recipient of the Outstanding graduate Student Member Award in IEEE St. Louis Section.



Hanfeng Wang (Student Member, IEEE) received the B.S. and M.S. degrees in electronic engineering from Tsinghua University, Beijing, China, in 2005 and 2008, respectively. He is currently working toward the Ph.D. degree with the Electromagnetic Compatibility Laboratory, Missouri University of Science and Technology, Rolla, MO, USA.

In 2008, he joined the Electromagnetic Compatibility Laboratory, Missouri University of Science and Technology. His current research interests include signal integrity, power integrity, and advanced numerical modeling.



Yansheng Wang (Student Member, IEEE) received the B.S. degree in electrical engineering from Beihang University, Beijing, China, in 2012. He is currently working toward the Ph.D. degree in electrical engineering with EMC Laboratory, Missouri University of Science and Technology, Rolla, MO, USA.

His research interests include radiation characterization for cable harness, method of moments, broadband H-field probe design, conducted emission modeling for switched-mode power supply, multiple-input multiple-output over-the-air testing, stochastic

modeling for high-speed channels, and generic models development for PCIe3/4.



Zhonghua Wu (Member, IEEE) received the B.S. degree in geophysics from the University of Science and Technology of China, Hefei, China, in 1989, the M.S. degree in geophysics from the Institute of Geophysics, Chinese Academy of Science, Beijing, China, in 1992, and the Ph.D. degree in electrical engineering from the State University of New York at Binghamton, Binghamton, NY, USA, in 1996.

He has been with Google Consumer Hardware Division, Mountain View, CA, USA, since 2012. He is one of the early contributors to USB Type-C

connector electrical specifications. He was with the Apple, Broadcom, Force10 Networks (part of Dell now), 3dfx (part of NVIDIA now), and LSI Logic. He specializes in signal and power integrity modeling, simulation and laboratory validation from PCB system to package and die levels.

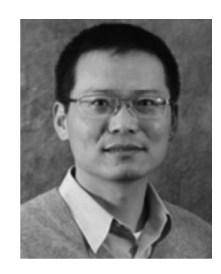


Chulsoon Hwang (Senior Member, IEEE) received the B.S., M.S., and Ph.D. degrees in electrical engineering from the Korea Advanced Institute of Science and Technology, Daejeon, South Korea, in 2007, 2009, and 2012, respectively.

From 2012 to 2015, he was with Samsung Electronics, Suwon, South Korea, as a Senior Engineer. In July 2015, he joined the Missouri University of Science and Technology (formerly University of MissouriRolla), Rolla, MO, USA, where he is currently an Assistant Professor. His research interests include

RF desense, signal/power integrity in high-speed digital systems, EMI/EMC, hardware security, and machine learning.

Dr. Hwang was a recipient of the AP-EMC Young Scientist Award, the Google Faculty Research Award, and Missouri S&T's Faculty Research Award. He was a corecipient of the IEEE EMC Best Paper Award, the AP-EMC Best Paper Award, and a two-time corecipient of the DesignCon Best Paper Award.



Jun Fan (Fellow IEEE) received the B.S. and M.S. degrees in electrical engineering from Tsinghua University, Beijing, China, in 1994 and 1997, respectively, and the Ph.D. degree in electrical engineering from the University of Missouri-Rolla, Rolla, MO, USA, in 2000.

From 2000 to 2007, he worked for NCR Corporation, San Diego, CA, USA, as a Consultant Engineer. In July 2007, he joined the Missouri University of Science and Technology (formerly University of Missouri-Rolla), and is currently a Professor and the

Director of the Missouri S&T EMC Laboratory. He also serves as the Director of the National Science Foundation Industry/University Cooperative Research Center for Electromagnetic Compatibility and a Senior Investigator of Missouri S&T Material Research Center. His research interests include signal integrity and EMI designs in high-speed digital systems, dc power bus modeling, intrasystem EMI and RF interference, PCB noise reduction, differential signaling, and cable/connector designs.

Dr. Fan served as the Chair of the IEEE Electromagnetic Compatibility (EMC) Society TC-9 Computational Electromagnetics Committee from 2006 to 2008, and was a Distinguished Lecturer of the IEEE EMC Society in 2007 and 2008. He currently serves as the Chair of the Technical Advisory Committee of the IEEE EMC Society, and is an Associate Editor for the IEEE TRANSACTIONS ON ELECTROMAGNETIC COMPATIBILITY and *IEEE EMC Magazine*. He received an IEEE EMC Society Technical Achievement Award in August 2009.